scientific reports

Check for updates

OPEN

Neonatal state and degree of necessity for parental care in *Maiasaura* based on inferred neonatal metabolic rates

Hugo Bert[1]✉, Holly Woodward[2], Nicolas Rinder[1], Romain Amiot[1], John R. Horner[3], Christophe Lécuyer[1], Mariana Sena[4] & Jorge Cubo[4]

We infer the neonatal metabolic rate at rest (RMR) and at maximum activity levels (MMR) of the hadrosaurid dinosaur *Maiasaura peeblesorum* from the Two Medicine Formation of Montana (USA) using Phylogenetic Eigenvector Maps applied to the following osteohistological features: the Relative Primary Osteon Area and the size of the femoral nutrient foramen as proxies. We investigate the locomotor/motor activity of the neonates by comparing the difference between maximum and minimum rates of oxygen consumption—referred to as aerobic scope and denoted as ΔMR, as a proxy of their activity levels. Applied to *Maiasaura*, this novel methodology allows for a quantitative assessment of its neonatal state and to deduce its dependence on parental care. The inferred neonatal RMR values for *Maiasaura* are similar to those of present-day fast-growing endotherms. As for the aerobic scope, *M. peeblesorum* neonates have a ΔMR value similar to those observed in present-day altricial birds that need intensive parental care. This result is consistent with the previously proposed hypothesis of nidicolous *M. peeblesorum* requiring parental care. Finally, based on age-estimations from *M. peeblesorum* neonate remains found both in and outside nest sites, we estimate that this species remained in the nest for approximately 40–75 days. *Maiasaura* provides a useful ecological baseline from which to infer neonatal states in an other hadrosaur of similar adult size—*Hypacrosaurus stebingeri*, whose differing ecological traits point to a relatively more precocial condition. The diversity of post-hatching reproductive strategy partly explains the adaptation of hadrosaurs to a wide range of paleolatitudes and environments.

Keywords Relative primary osteon area, Nutrient foramina, Phylogenetic eigenvector maps, Reproductive strategy

The time and energy invested by parents in post-natal care in tetrapods partly control reproduction rates and offspring survival rates, two key parameters used in models to explain population dynamics and dispersion[1–4]. Post-natal parental care is thus a key factor in the understanding of the biogeography of a species and its evolutionary history[2,5,6]. However, post-natal parental care (food provision, protection against predation, grooming) is difficult to infer in extinct tetrapods as it leaves scarce traces in the fossil record[7]. Post-hatching parental care has been proposed for the ornithischian dinosaur *Psittacosaurus* based on the exceptional discovery of an adult closely associated with 34 juveniles interpreted as its offsprings[8]. It was also proposed for the saurolophine hadrosaur *Maiasaura peeblesorum* based on the cartilaginous long bone epiphyses of the hatchlings suggesting a neonatal lack of locomotor activity[7] and the exceptional discovery of 11 juveniles of a few months old that died in their nest, suggesting that there were nestlings[9]. More indirectly, nest building and brooding behavior identified for instance in some oviraptorid theropods[10], or the coexistence of several ontogenetic stages in the same herd inferred from hadrosaurid track sites[11] also supported the hypothesis of parental care in non-avian dinosaurs. On the contrary, the lambeosaurine hadrosaur *Hypacrosaurus* is recovered

[1]Laboratoire de Géologie de Lyon: Terre, Planètes, Environnement, UMR CNRS 5276, Université Claude Bernard Lyon 1, ENS de Lyon, 2 Rue Dubois, 69622 Villeurbanne, France. [2]Oklahoma State University Center for Health Sciences, 1111 W 17th St, Tulsa, OK 74107, USA. [3]Schmid College of Science and Technology, Chapman University, Orange, CA 92866, USA. [4]Muséum National d'Histoire Naturelle, CNRS, Centre de recherche en paléontologie –Paris (CR2P, UMR 7207), Sorbonne Université, 4 Place Jussieu, BC 104, Paris, France. ✉email: hugo.bert@univ-lyon1.fr

in age-segregated herds in the deposits based on long bone histology[12]. It was suggested that these dinosaurs were precocial and thus have been able to survive without parental care. On the other hand, intensive parental care due to the lack of mobility in *M. peeblesorum* has been challenged based on the fully mineralized pelvis of the neonates enhancing a neonatal locomotor capacity as well as on the absence of adult skeletal remains at nest sites[13].

The classification of Nice[14] for present-day birds associates the degree of post-hatching parental care with the state of the neonates in the altricial-precocial spectrum, with intensive parental care given to altricial neonates. The neonatal state could be quantitatively represented by the neonatal aerobic scope noted ΔMR value, corresponding to the difference between the maximum and the minimum rates of oxygen consumption. As they have locomotor and motor systems inactive, altricial species stay in the nest for an extended period and are characterized by a maximal metabolic rate (MMR) equal to the resting metabolic rate (RMR) (ΔMR = 0)[15]. On the contrary, precocial bird species are able to forage alone at hatching and consequently have a higher MMR value than their RMR one (ΔMR > 0). This rule is less true in shorebirds like the brush-tailed penguins *Pygoscelis* or representatives of the Scolopacidae that live in cold and windy environments inducing a very high energetic cost at rest, hence reducing their ΔMR values[15,16]. It does not apply to hyperprecocial ectothermic reptiles like sea turtles or crocodiles that mostly rely on anaerobic power even at peak activity, also leading to reduced or null ΔMR value[17,18]. Compared with altricial species, parental care is reduced or absent in precocial species. In ducks, neonates are autonomous but stay near their parents[14,15]. In megapodes, neonates hatch without the parents and survive alone[19].

The aim of this study is to infer neonatal mass-specific RMR and MMR values of *M. peeblesorum* from the middle and late Campanian of the Two Medicine Formation (82–76 My[20]) in order to calculate its neonatal ΔMR value. This metabolic scope provides the first quantitative insight into the position of this ornithischian dinosaur in the altricial-precocial spectrum by comparing it with those of extant tetrapod species. The result allows for a qualitative hypothesis regarding the degree of dependence to parental care in *Maiasaura*. Analyzing this duck-billed dinosaur as a case study is appropriate as a first attempt at this method because it is represented in the fossil record by embryonic/perinatal remains, sometimes associated with nests and eggs[21], enabling accurate data to be collected.

We infer the neonatal mass-specific MMR and RMR values using phylogenetic eigenvector maps (PEM)[22–26], a statistical tool designed to build models integrating phylogeny and considering phylogenetic information as a weighted influence matrix. The models are built with metabolic rate data from extant species, their osteo-histological variables and a set of phylogenetic eigenvectors used as predictors[22,23,27]. We used the femoral relative density of primary osteon (RPOA) as an explanatory variable for RMR. In juveniles, the resting metabolic rate is primarily correlated with bone growth rate[27], which is characterized by vascularization during mineralization represented by RPOA[28–31]. We used blood flow as an explanatory variable for MMR. Femoral blood flow is correlated with MMR because it is related to bone oxygen supply[32] for bone remodeling due to stresses of locomotion and vary similarly to the oxygen consumption of animals running on treadmills[33,34].

We then discussed the significance of the estimated ΔMR value in terms of neonatal state and its ecological implications based on present-day birds and mammals[15,35,36]. This novel method can subsequently be applied to other extinct tetrapod species.

Material and methods

Material

Material

This study is based on the analysis of 23 femora attributed to the saurolophine *M. peeblesorum* recovered from the Campanian in Montana, USA, and curated at the Museum of the Rockies (MOR) or Princeton University (YPM-PU) (listed in Table 1). They include 4embryonic long bones (2 femora, 1 tibia, and 1 humerus)[21], and long bones representing a large proportion of all other postnatal ontogenetic stages as presumed based on their femoral circumference and lenght (Fig. 1, Table 1). Two other specimens (MOR 758 16-16-15-99 presented Fig. 2 and MOR PU 22400 GS400F3 presented in supplementary material 6) are mid-diaphyseal femoral thin sections that still contain embryonic bone. Fossils of *M. peeblesorum* were previously collected between the two bentonite levels Hadro Hill 8-9-93 dated 78.6My and L2R061517-1 dated 76.2My[20].

We modeled the ontogenetic evolution of the femoral nutrient foramen radius (R) in *Maiasaura* with the evolution of femoral mid-shaft circumference (Fc) representing the developmental stage (Table 1, Fig. 1E). The equation is a power function having the following shape: $Y = aX^b$, accordingly to previous studies about distribution of blood flow with adult body mass, or through the ontogeny[18,33,37].

We also used 14 neonates from present-day species of mammals, birds amphibians, crocodiles, turtles and lizards listed in Table 2 to build a model for neonatal mass-specific RMR inferences.

We obtained the necessary permissions to study each specimen from their original collections (see Data Availability for details on the scanned specimens. *Rangifer tarandus*: Museum National d'Histoire Naturelle, la collection des mammifères; *Pygoscelis_adeliae*, *Anas sp.*: Museum National d'Histoire Naturelle, la collection des oiseaux; *Larus glaucescens*: Oklahoma State University).

Methods

CT-scan and 3D models

Bones were CT-scanned with a Double Tomograph at High Energy (DTHE) from RX Solutions. Regarding the fossil material, we used a current of 103.4 µA and a voltage of 180 kV and a voxel size of 13–16 µm (supplementary material 1). Regarding the extant specimens, we tested their preservation fluid for the presence of formaldehyde using Schiff's reagent to ensure that the tissues were properly fixed and could withstand further treatments. The specimens were then washed 3 times in baths composed of a 70%-alcohol-30%-water mixture to ensure a good

Collection number	Fc (mm)	Fl (mm)	NFA (mm^2)	Blood flow (mL/min)	References/comments
MOR 547 W-16-4	164	486	3.90	0.657	This study
MOR 547 W-27-1	149	**444**	4.28	0.731	This study
MOR 547 W-17-7	178	520	4.80	0.834	This study
MOR 240 2024-c-243	18	**44**	0.16	0.014	This study, embryo
MOR 240 2024-c-238	22	**51**	0.07	0.005	This study, embryo
MOR 005 2023-c-207	297	**855**	33.89	7.074	This study
MOR 005 33094	159	**456**	1.70	0.250	This study
MOR 005 33063	155	**447**	2.99	0.483	This study
MOR 005 2023-c-208	275	793	18.12	3.673	This study
MOR 758 NC-9-13-98-84	278	**801**	20.24	4.090	This study
MOR 758 NC-9-13-98-84	277	**798**	20.27	4.097	This study
MOR 005 1990	277	798	18.31	3.673	This study
MOR 005 (no collection number)	167	428	11.03	2.113	This study
MOR 005 1988	192	**553**	14.97	2.953	This study
MOR 005 7-12-91-44	292	**841**	22.54	4.590	This study
MOR 1002	32	76	0.17	0.014	Data from[18]
YPM-PU22400 fm-(1)	47	123	0.25	0.023	Pictures from Prieto-Marquez et al., (2018)
YPM-PU22401 fm-(5)	54	133	0.31	0.031	Pictures from Prieto-Marquez et al., (2018)
MOR 005 (no collection number)	49	**116**	0.25	0.024	This study
MOR 240 2024-c-241	19	–	0.32	0.033	This study, tibia, embryo
MOR 240 2024-c-239	22	–	0.15	0.013	This study, humerus, embryo

Table 1. *Maiasaura* specimens used to model the evolution of femoral nutrient foramen dimensions in relation to the evolution of femoral circumference. Collection number, femoral circumference Fc, femoral length Fl (for broken bones, femoral length was estimated using a cross product based on complete femora of similar size. These estimations are written in bold), nutrient foramen area NFA, and blood flow of hadrosaurid taxa. Blood flow estimations were determined based on the nutrient foramen radius calculated from their area, following[37]. MOR specimens come from the Museum of the Rockies and YPM specimens are published specimens from theYale Peabody Museum of Natural History.

contrast between bone and flesh on the slides. These specimens were scanned out of their preservation fluids with a current ranging from 80 to 263 µA and a voltage ranging from 100 to 200 kV and a voxel size ranging from 9 to 25 µm (see supplementary material 1 for details). Volume rendering, processing of scans (femur or nutrient foramen) and measurements were obtained using Avizo software (Avizo 3D Lite 9.2, ThermoFischer Scientific). The 3D models are digitally stored in their respective collections (supplementary material 1).

Phylogenetic eigenvector maps

Both maximal and resting metabolic rates were inferred using phylogenetic eigenvector maps (PEM ; supplementary material 2; e.g.[23,25,26]) on R (4.3.0) [38]. It is a predictive modeling technique for missing data that considers phylogenetic non-independence[24] (supplementary material 3). A calibrated tree for present-day taxa is coded as a matrix that is transformed to extract eigenvectors. Two parameters control the extent of the evolutionary changes along the branches: 1) "a" ($0 < a < 1$) representing the steepness of the evolutionary changes after each phylogenetic node that is estimated with the "PEM.fitSimple" function of the "MPSEM" R package[24] and 2) "Ψ" representing the relative evolutionary rates[23,24,39]. We assumed that metabolic rates evolved constantly throughout the phylogeny[23]. We thus assigned a single pair of "a" and "Ψ" value per model. When $a = 1$, evolution occurs at fixed rates independently of branch lengths. When $a = 0$, changes occur in proportion to the square root of branch length. The values used for inferences were intermediate, with 0.425 for MMR models and 0.419 for RMR models. Regarding Ψ, we choose the default value of 1 following Molina-Venegas et al.[39]. n-1 eigenvectors are produced, n the number of taxa used in a model. The functions lmforwardsequentialsidak or lmforwardsequentialAICc in MPSEM performed a forward stepwise selection of these eigenvectors[24]. We produced two models: a first model accounting for the phylogeny and the evolution of the response variable (to be inferred in the hadrosaur species) and a second including in addition a predictor variable (a bone histological or osteological feature).

The widespread lmforwardsequentialAICc function use the corrected Akaike information criterion (AICc)[40] to find the best model having the lowest AICc value and the highest R^2 value. It produces a model that minimizes overfitting while optimizing the balance between fitting quality and complexity. However, it has been shown that the AICc approach displayed high type I error and resulted in wrong ecological interpretation[41]. The lmforwardsequentialsidak function used the Holm-Sidak correction[24,42,43] to find a model that controls the type I error and minimizes the risk of false significance. In this study, the authors prefer the Holm-Sidak correction selection procedure over AIC selection procedure, but we propose to compare the results of both methodologies (supplementary material 8. A. and B.).

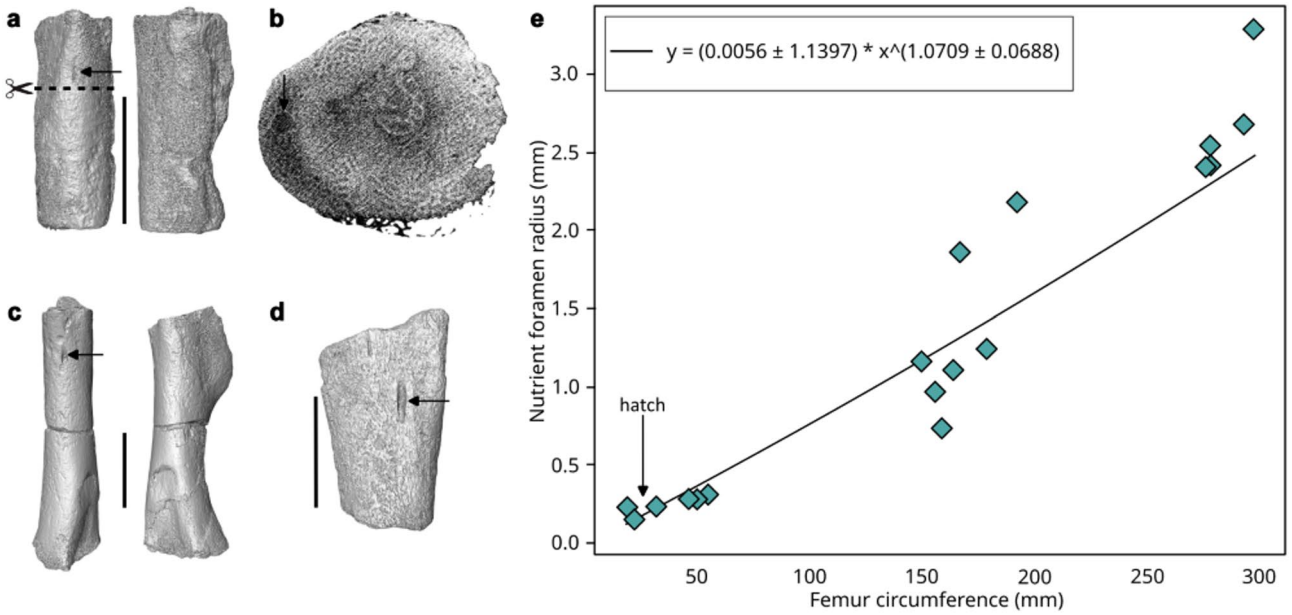

Fig. 1. Ontogenetic evolution of the femoral nutrient foramen radius. (**a–d**) *M. peeblesorum* 3D models from the embryonic MOR 240 2024-c-238 (femur), MOR 240 2024-c-241 (tibia), and MOR 240 2024-c-239 (humerus)[21], black and white arrows point to the nutrient foramen, the scale bar represents 1 cm. (**a**) Femur in anterior and lateral? view. (**b**) Femoral section of the 3D model. (**c**) Humerus in anterior and lateral or medial view. (**d**) Tibia. (**e**) Ontogenetic evolution of the nutrient foramen radius in mm with the mid-shaft circumference of the femur in mm (Table 1). 3D models were obtained with Avizo 3D Lite 9.2, ThermoFischer Scientific and are available upon request from the Museum of the Rockies.

A model was accepted only if its residuals followed a normal distribution, i.e., if the p-value obtained from the Shapiro–Wilk normality test on the residuals was greater than 0.05[44].

The initial models for RMR and MMR inferences yielded residuals that did not follow a normal distribution with *p*-values of 0.023 and 0.014 respectively. We consequently discarded these two first models and a log-transformation was applied to both RMR and MMR values, as recommanded by[23]. Nonetheless, explanatory variables were not log-transformed to avoid issues with zero values. Following the transformation, the Shapiro–Wilk test yielded p-values of 0.67 and 0.38 for RMR and MMR respectively, leading to the acceptance of the models for RMR and MMR inferences. Further in this study, the results are presented in their exponential form to reverse the log transformation. We finally checked the predictive power of the model by performing a leave-one-out cross-validation test (supplementary material 8. B.).

Histological and osteological variables

Nomenclature

We followed the nomenclature of de Buffrénil and Quilhac (2021)[45] to describe bone histological structures.

Relative primary osteon area

We used the relative primary osteon area (RPOA) defined as the surface occupied by the primary osteons divided by the observed surface[31] as an explanatory variable for neonatal mass-specific RMR. In juveniles, RMR is primarily correlated with bone growth rate[27], which is characterized by vascularization during mineralization as blood primarily supply osteocytes in oxygen[28–30,32]. RPOA is thus a proxy for the oxygen needs during bone formation[31,45], and is therefore correlated with RMR[31].

RPOA measurements were conducted on the two *M. peeblesorum* femoral sections MOR 758 16-16-15-99 and MOR PU 22400 GS400F3 exhibiting a neonatal line and therefore an innermost cortex representative of the postnatal condition (supplementary material 6). Embryonic bone is extensively resorbed in MOR PU 22400 GS400F3.

Bone sections were studied using the Nikon Optiphot2-POL microscope from the Museum of the Rockies coupled with a Nikon DS-Fi-2 camera. We used the NIS-Elements BR 5.21.03 software (Nikon Imaging Software-Elements Basic Research) to produce mosaic images of the entire femoral sections (e.g. Fig. 2A, B). Under lambda wave plate, the primary osteons are composed of birefringent lamellar or parallel-fibered bone[46]. The primary osteons are delimited by the isotropic woven bone presenting a higher density of osteocyte lacunae[46].

The delimitation of the primary osteons and the calculation of their density were made manually using a graphic tablet (Wacom Cintiq 22) and the ImageJ 1.54 k software. Measurements were taken as close as possible to the neonatal line in order to observe the perinatal conditions.

Blood flow

Blood flow (Q) is the volume of blood perfusing the femur per time unit and can be computed using the Eq. (1).

$$\mathrm{Log}\ \left(\dot{\mathrm{Q}}\,\mathrm{ml\ min}^{-1}\right) = -0.20.\log\left(\mathrm{r}\right)^{2} + 1.91.\log\left(\mathrm{r}\right) + 1.82 \quad (1)$$

with r the radius of the femur nutrient foramen[47]. Equation (1) was built using mammals but has also previously been applied to *Maiasaura*[18]. We used it as an explanatory variable for mass-specific MMR (e.g.[26]), because bone perfusion is related oxygen supply[32] for bone remodeling upon microfractures due to exertion, and to the ability to withstand blood pressure[48]. In fact, blood flow and MMR covary with body mass, both following a relationship involving the same exponent[33,47]. Nutrient foramina are bone openings through which an artery enters from the external bone surface to supply cortical bone with blood[49]. In mammals, a perforating branch of the deep femoral artery passes through the nutrient foramen and fills 50–70% of the foramen[50]. Some bird species have pneumatized long bones with both an air sac and an artery passing through the pneumatic foramen, reducing the femoral artery space to 20% of the foramen volume[51]. As we do not know the space occupied by the femoral artery in dinosaur femoral nutrient foramen, we decided to use *r* as the radius of the nutrient foramen rather than the radius of the artery following[26].

We measured the nutrient foramen in 19 *M. peeblesorum* femora of different ontogenetic stages, including the two *M. peeblesorum* embryos MOR 240 2024-c-243 and MOR 240 2024-c-238 (Table 1, Fig. 1E). The nutrient foramen is funnel-shaped and measurements were taken using ImageJ software following the methodology proposed in[33]. Measurements of embryos were taken on 3D models (Fig. 1A,B). The foramen radius was turned into Q following the polynomial Eq. (1) of[47] for apneumatic femora that was calibrated on 20 species of present-day mammals. We also studied the two 3D models of embryonic *M. peeblesorum* MOR 240 2024-c-241 (tibia) and MOR 240 2024-c-239 (humerus) in order to compare the dimensions of their nutrient foramen with those of the two *M. peeblesorum* embryonic femora (Fig. 1A–D).

Models for neonatal metabolic rate inference

The model for neonatal resting metabolic rates inference

Mass-specific RMR is very dynamic through ontogeny, especially during early development with body mass increasing asymptotically (e.g.[15]). To avoid possible ontogenetic biases, we built a new dataset that represents as much as possible neonatal conditions for inferring neonatal metabolic rates. The dataset was built based on the present-day species previously used in[22] which complements the dataset proposed in[27]. Age of the growing specimens were estimated based on their body mass and their specific growth rate provided in[27]. We estimated ages ranging from 5 to more than 100 days. To better fit with neonatal conditions, we replaced when possible RMR values measured in[27] with neonatal RMR values (0–4 days) available in the research literature (See supplementary material 5 A. and B. for details). As expected due to the stresses associated with birth or hatching, we observed resting metabolic rate in neonates higher than those of juveniles (e.g.[16,38]). No age estimation could have been made on *Alligator mississippiensis* and *Caiman crocodilus*, and ages higher than a month were estimated for the species *Chelodina oblonga*, *Pelodiscus sinensis*. As no neonatal RMR value were available in the literature for these four species, they were consequently discarded from the dataset. Finally, the 15 remaining species (See Table 3) have RMR values corresponding to 0–10 days (see Table 3). Despite the fact that ontogenetic temporality differs from one species to an other, we estimated that such dataset yet offers the best balance between the number of taxa and the accurate representation of neonatal conditions. We used the RPOA measurements from[24], taken from the innermost cortical region of juvenile specimens, as these are the most representative of postnatal conditions in the available research literature. The model finally includes: 1 amphibian, 1 turtle, 2 birds, 6 mammals, 1 crocodile, and 4 lizards (Table 3, supplementary material 5).

The model for maximal metabolic rate inference

No dataset for neonatal maximal metabolic rate inferences was available before this study, or for neonatal blood flow estimation based on femoral nutrient foramen radius. The existing data were acquired from adults[26] and their use for neonatal estimation could be skewed by ontogeny. We therefore established a dataset that is limited by the availability of neonatal MMR values (within the 5 first days of life) in the litterature and the number of neonate species available in museum collections. The final dataset includes neonates from 16 present-day species (Table 2, supplementary material 4 and 7 for the references). The dataset also excluded all bird species having air sacs in their femora which skewed the estimations of the dimension of the foramen[52–54]. The nutrient foramen radius was calculated from nutrient foramen area measurements. The dataset for MMR finally includes: 1 crocodilian, 1 mammal, 1 varanid, 2 turtles, and 11 birds (Table 2, supplementary material 4 and 7).

Unit

Previous studies using the PEM expressed metabolic rates in $mL_{(O2)}\ h^{-1}\ g^{-0.67}$[22,25,26]. The allometric mass scaling exponent 0.67 accounts for the caloric losses linked to the decrease of the ratio surface/volume with increasing body mass. It was first determined theoretically by euclidean surface-area-to-volume considerations[64]. Empirical studies show that the theoretical 0.67 exponent does not fit current observations (e.g.[65]). The empirical allometric exponent may vary from 0.67 to 1 depending on the group, the thermophysiology, the ontogenetic stage, the activity (rest, activity, stress, etc.) and the environment (temperature, food, etc.) (e.g.[37,66,67]). As we cannot use different exponents for different taxonomic groups in a given analysis, we expressed in this study the metabolic rates using the allometric exponent of 0.67 so that (1) the units are homogeneous despite the type of organism and (2) the inferred metabolic rates are comparable with previous data resulting from PEM analysis.

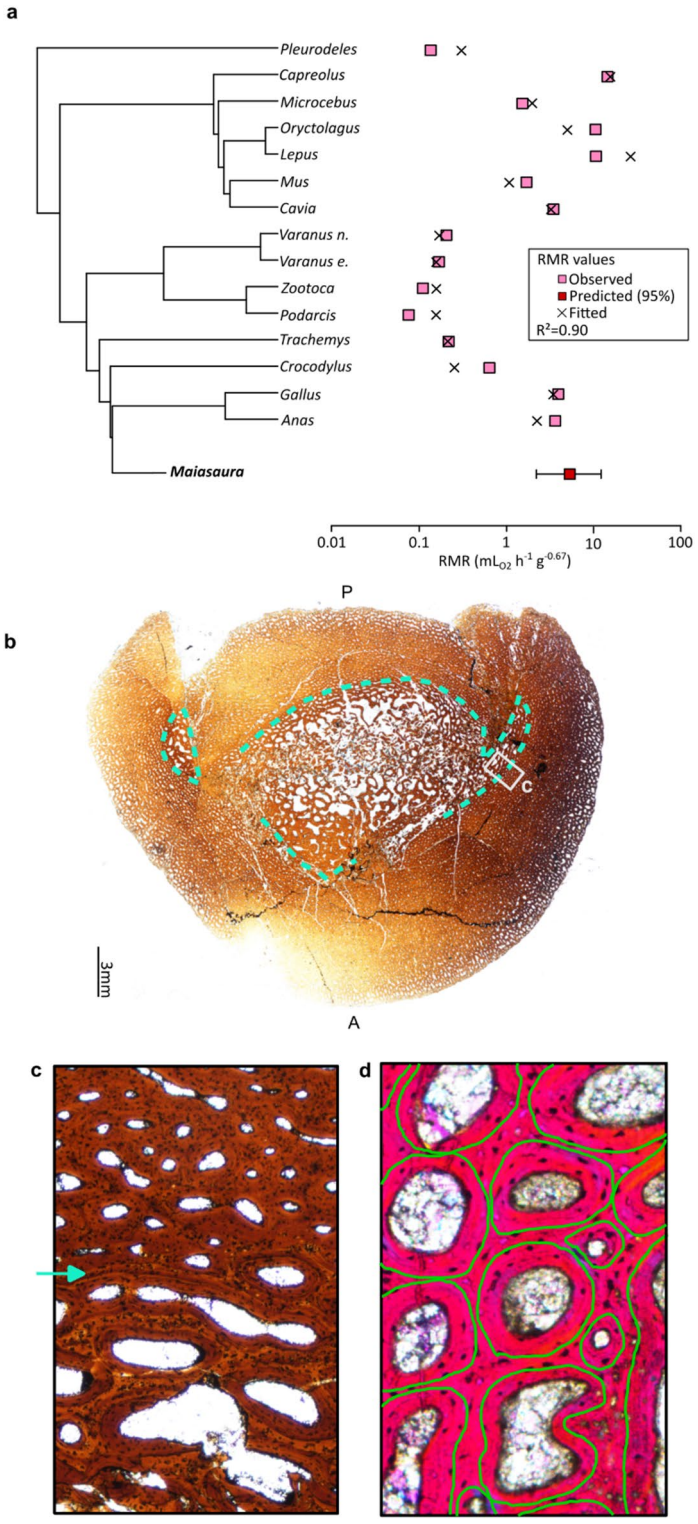

The error associated with environmental factors may be minimized, as metabolic rate values were obtained from laboratory measurements conducted under standardized environmental conditions[15,17,27,60,68].

Phylogenetic relationships

Phylogenetic relationships were coded as typology and branch lengths, with branch lengths being the age separating two successive nodes or node and terminal taxon.

The phylogeny of extant species used to build models for RMR inferences was taken up from[25,69–71] to build models for RMR inferences (supplementary material 3). We used the same phylogeny as much as possible to build models for MMR inferences and we detailed turtle phylogeny following[72], and bird phylogeny following[73,74] (supplementary material 3)..

◀**Fig. 2**. Neonatal RMR inferences using PEM and the neonatal RPOA value as co-predictor. (**a**) Results of the PEM analysis using RPAO as a predictor variable for RMR inferences in $mL_{(O2)}\ h^{-1}\ g^{-0.67}$. Fitted values are available in the supplementary material 8. B. The black dots are the osteocytes lacunae. The RPOA value of 0.74 equals the area delimited by the green outlines divided by the total area delimited with the black rectangle. (**b**) Femoral thin section under natural light of the hatchling MOR 758 16-16-15-99 (right) that has been slightly crushed anteroposteriorly during diagenesis. The area delimited in blue corresponds to the embryonic area. A and P the anterior and posterior parts. The blue dashed lines indicate the neonatal line. The black dots are the osteocytes lacunae. The RPOA value of 0.74 equal the area in green divided by the total area delimited with the black rectangle. (**c**) Zoom under natural light in the black rectangle in b to show the neonatal line (blue arrow) delimited by drastic change of vascularization. Embryonic bone to the Left, cortex to the right. (**d**) RPOA measurement on the cortex area with lambda wave plate. The calcite in white fills the primary osteon delimited in green[46]. The black dots are the osteocytes lacunae. The RPOA value of 0.74 equal the area in green divided by the total area delimited with the black rectangle.

Species	Collection number	Observation	R (mm)	Q (ml min^{-1})	Species	MMR ($mL_{O2}\ h^{-1}\ g^{-0.67}$)
Rangifer tarandus	1940-172 (MNHN)	direct	0.35	0.0400528	*Rangifer tarandus*	45.67
Crocodylus niloticus	Cr.0056-107 (MNHN) AgSVSTUA022002 (ENS)	CT-scan	0.10	0.0015849	*Crocodylus niloticus*	0.88
Pygoscelis papua	1913-486 (MNHN)	direct	0.13	0.0029609	*Pygoscelis papua*	5.89
Pygoscelis papua	–	–	–	–	*Pygoscelis antarctica*	6.70
Pygoscelis papua	–	–	–	–	*Pygoscelis adeliae*	5.40
Anas sp.	1880-171 (MNHN)	direct	0.15	0.0045411	*Anas crecca*	20.40
Anas sp.	–	–	–	–	*Anas platyrhynchos*	18.57
Varanus niloticus	LF4 (UCBLZ) Va.0012-80 (MNHN)	CT-scan	0.06	0.0003865	*Varanus niloticus*	6.54
Chelonia mydas	agSVSTUA022008 (ENS) Chelonia mydas (UCBLZ)	CT-scan	0.04	0.0000837	*Dermochelys coriacea*	1.15
Lepidochelys olivacea	To.0516-11 (MNHN)	CT-scan	0.02	0.0000108	*Lepidochelys olivacea*	0.85
Larus glaucescens	OMNH RE 887 (Oklahoma State University)	direct	0.19	0.0086662	Larus occidentalis	10.80
Larus glaucescens	–	–	–	–	*Larus dominicanus*	8.54
Psittacula krameri	Z2018.01.438.1 (UCBLZ)	CT-scan	0.06	0.0003881	*Nymphicus hollandiscus*	2.83
Procellaria aequinoctialis	MNHN-ZO-2021–3036	CT-scan	0.13	0.0028890	*Procellaria aequinoctialis*	11.32
Procellaria aequinoctialis	–	–	–	–	*Procellaria cineria*	12.20
Ara ararauna	NMB 29.9.62	CT-scan	0.06	0.0007488	*Ara ararauna*	4.04

Table 2. Neonatal blood flow (Q) estimated based on the femoral nutrient foramen radius (R) of neonates from 14 present-day vertebrate species and associated neonatal mass-specific MMR values used to construct a model for neonatal mass-specific MMR inference. All specimens are 0 to 4 days old (supplementary material 4). We extrapolated the Q value for specimens of the same genus with similar neonatal body mass and neonatal stage. MMR values were taken within the data available from the literature (See supplementary material 4 and 7).

The phylogenetic relationship between *M. peeblesorum* and the present day species was taken in Langer et al.[75], and the datation of *Maiasaura* was taken from Rogers et al.[20].

Results

Neonatal relative primary osteon area measurements

We found a RPOA value of 0.74 ± 0.07 (MOR PU 22400 GS400F3) and of 0.76 ± 0.05 (MOR 758 16-16-15-99) with a mean value of 0.75 ± 0.05 for the innermost cortex of the two hatchling *M. peeblesorum* (Table 4). The uncertainties are standard deviations calculated with RPOA values measured in the anterior, posterior, lateral and medial parts of the thin sections.

Neonatal blood flow estimation

Femoral circumference, length, nutrient foramen area measurements, and blood flow estimations are listed in Table 1 for 19 *M. peeblesorum* specimens (We have not included the embryonic tibia and humerus in the model). Data for one *M. peeblesorum* tibia and humerus perinatal/embryonic specimens are also given.

We modeled the ontogenetic evolution of the femoral nutrient foramen radius (R) with the evolution of femoral mid-shaft circumference (Fc) representing the developmental stage (Table 1, Fig. 1E). We obtained the Eq. (2).

Species	RPOA	RMR ($mL_{O2}\ h^{-1}\ g^{-0.67}$)	Age of RMR measurements (days)	Reference for neonatal RMR values
Pleurodeles waltl	0.00	0.14	0 (newt)	[55]
Capreolus capreolus	0.74	14.45	0	[56]
Microcebus murinus	0.24	1.53	9	[57]
Cavia porcellus	0.34	3.48	5	[27]
Mus musculus	0.08	1.71	10	[27]
Lepus europaeus	0.81	10.67	4	[58]
Oryctolagus cuniculus	0.42	10.51	4	[59]
Zootoca vivipara	0.00	0.11	7	[57]
Podarcis muralis	0.00	0.08	7	[27]
Varanus exanthematicus	0.01	0.17	0	Estimated from[60]
Varanus niloticus	0.02	0.21	0	Estimated from[60]
Trachemys scripta	0.00	0.22	4	[61]
Crocodylus niloticus	0.05	0.63	0	[62]
Anas platyrhynchos	0.58	3.62	0	[63]
Gallus gallus	0.68	3.95	0	[63]

Table 3. RPOA and neonatal mass-specific RMR values of 15 present-day species used to construct a model of mass-specific RMR inference. RPOA values come from[24]. RMR values were extracted from published data (See the references in supplementary material 5).

Collection number	RPOA	Comments
MOR 758 16-16-15-99	0.76 ± 0.05	Secondarily flattened. Embryonic bone and cortex
MOR PU 22400 GS400F	0.74 ± 0.07	Embryonic bone extensively resorbed and cortex

Table 4. RPOA values measured on mid-diaphysis femoral sections.

RMR ($mL_{(O2)}\ h^{-1}\ g^{-0.67}$)	MMR ($mL_{(O2)}\ h^{-1}\ g^{-0.67}$)	ΔMR ($mL_{(O2)}\ h^{-1}\ g^{-0.67}$)
lmforwardsequentialsidak		
$5.2_{2\to12}$	$6.0_{4\to9}$	$0.8_{0\to9.5}$
lmforwardsequentialAICc		
$6.3_{3\to13}$	$7.0_{5\to10}$	$0.7_{0\to9.5} \pm 7.5$

Table 5. Metabolic rate inferences using the forward stepwise eigenvector selection using Holm–Sidak correction (sidak)[42,43] and the corrected Akaike Information criterion (AICc)[40] with the MPSEM R package[24,38]. The results are presented graphically in SM 8.

$$R = 0.0056 \pm 1.13974 \ * \ Fc^{1.0709 \pm 0.0688}\ (n = 21)\,. \tag{2}$$

We estimated *M. peeblesorum* embryonic femoral circumference based on measurements of the embryonic region of its mid-diaphysis femoral sections (MOR PU 22400 GS400F3 and MOR 758 16-16-15-99) using the software ImageJ (Fig. 2A). Following the neonatal line, we estimated a maximal mean embryonic femoral circumference of about 25.53 mm.

Applying the Eq. (2) (Fig. 1E), we determined nutrient foramen radii of 0.180 for *M. peeblesorum* corresponding to blood flows of 0.007564 using Eq. (1).

Inferred neonatal metabolic rates

Results are presented in Table 5.

With the Holm–Sidak selection procedure, we obtained a neonatal mass-specific RMR value of $5.2_{2\to12}$ $mL_{(O2)}\ h^{-1}\ g^{-0.67}$ for *M. peeblesorum* using RPOA as an explanatory variable (Fig. 2, Table 5). We used the default alpha value of 0.05 of lmforwardsequentialsidak for the selection procedure. This model including the RPOA as a predictor variable has a R^2 of 0.90, a p-value of $3.97^{*}10^{-7\cdot}$. It has a better fit than a model built without the additional explanatory variable ($R^2 = 0.53$).

Neonatal mass-specific MMR value were determined for *M. peeblesorum* integrating blood flow as a predictor variable. The default sidak selection procedure (alpha = 0.05) was too restrictive and produced a model with an insufficient fitting (with alpha = 0.05, $R^2 = 0.33$). We used an alpha-value of 0.20 instead of 0.05, allowing the selection of an additional eigenvector to build the model. The risk of type I error increased to 20% instead of 5%, which is still lower than the risks of 100% produced with an AIC selection procedure[41].

Neonatal mass-specific MMR values of $6.0_{4\to9}$ $mL_{(O2)}$ h^{-1} $g^{-0.67}$ were determined for *M. peeblesorum* (Fig. 3, Table 5). This model ($R^2 = 0.77$, p-value = $9.672^{*}10^{-5}$) has a better fit than the one built without the additionnal explanatory variable ($R^2 = 0.37$).

With the AIC selection procedure, we obtained a neonatal mass-specific RMR value of $6.3_{3\to13}$ $mL_{(O2)}$ h^{-1} $g^{-0.67}$ for *M. peeblesorum* (Table 5). This model including the RPOA as a predictor variable has a R^2 of 0.93, an AIC of 30, and a p-value of 3.306e−07. It has a better fit than a model built without the additionnal explanatory variable ($R^2 = 0.53$, AIC = 40).

Neonatal mass-specific MMR values of $7.0_{5\to10}$ $mL_{(O2)}$ h^{-1} $g^{-0.67}$ were determined for *M. peeblesorum* integrating blood flow as a predictor variable (Table 5). This model ($R^2 = 0.99$, AIC = 2, 1.554e−08) has a better fit than the one using the phylogeny built without the additionnal explanatory variable ($R^2 = 0.98$, AIC = 17).

Difference between neonatal maximum and resting metabolic rates (ΔMR)

Neonatal ΔMR values for present day species were calculated in this study using data available from the literature (Fig. 4, Table 6). The mean neonatal *M. peeblesorum* ΔMR value is of $1_{0\to9}$ $mL_{(O2)}$ h^{-1} $g^{-0.67}$ ($X_{0\to uncertainty}$ is a notation to avoid impossible negative ΔMR values) whether the eigenvector selection method used is AICc or sidak selection procedure. This mean ΔMR value falls within the range of altricial birds and hyperprecocial ectotherms.

Discussion

Selecting the eigenvectors

We compared models obtained using forward stepwise selection of eigenvectors of the MPSEM R package[24]. The criteria of selection of the eigenvectors could be based on AICc[40] or Holm-Sidak correction[42,43]. AICc is routinely used in Phylogenetic Eigenvector Maps (PEM) e.g.[22,23,25,26], and is a method minimizing overfitting and optimizing fitting and complexity. However, it has been shown that this methodology is sensitive to Type I error[41]. Consequently, the selection can be skewed, as well as the physiological interpretation resulting from the

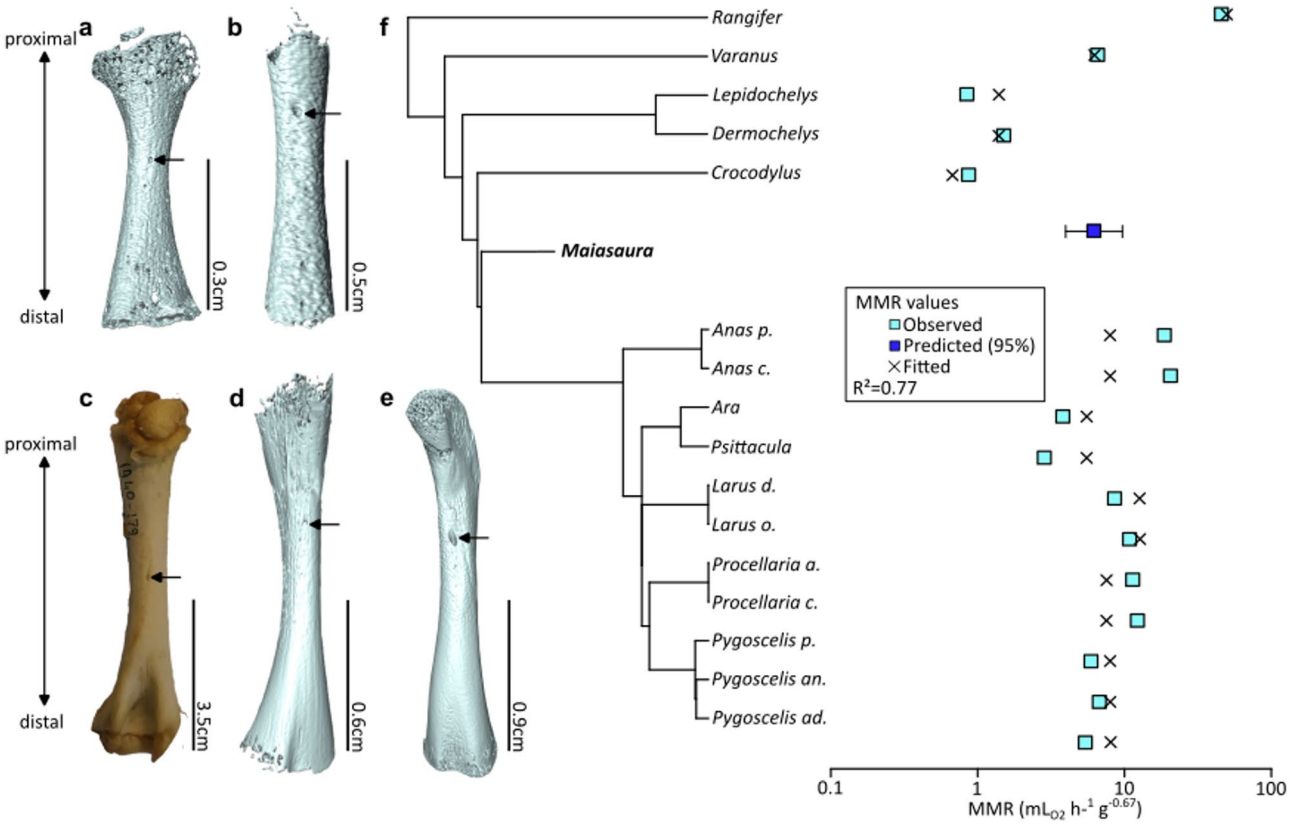

Fig. 3. Neonatal MMR inferences using PEM and the neonatal blood flow as co-predictor. (**a**–**e**) Localization of the nutrient foramen in present-day neonates, the arrows point to the foramen. Epiphyses are not always mineralized. (**a**) 3D model of a femur of the neonate *Chelonia mydas* ENS-AgSVSTUA022002. (**b**) 3D model of a femur of the neonate *Procellaria aequinoctialis* MNHN-ZO-2021-3036. (**c**) Photograph of a femur of the neonate *Rangifer tarandus* MNHN-1940–172. (**d**) 3D model of the femur of a neonate *Varanus niloticus* MNHN-Va.0012-80. (**e**) 3D model of a femur of the neonate *Crocodilus niloticus* MNHN-Cr.0056-107. (**f**) Results of the PEM analysis using blood flow as a predictor variable for MMR inferences in $mL(O_2)$. $h^{-1}{\cdot}g^{-0.67}$[22,23,25]. Fitted values are available in the supplementary material 8. B.

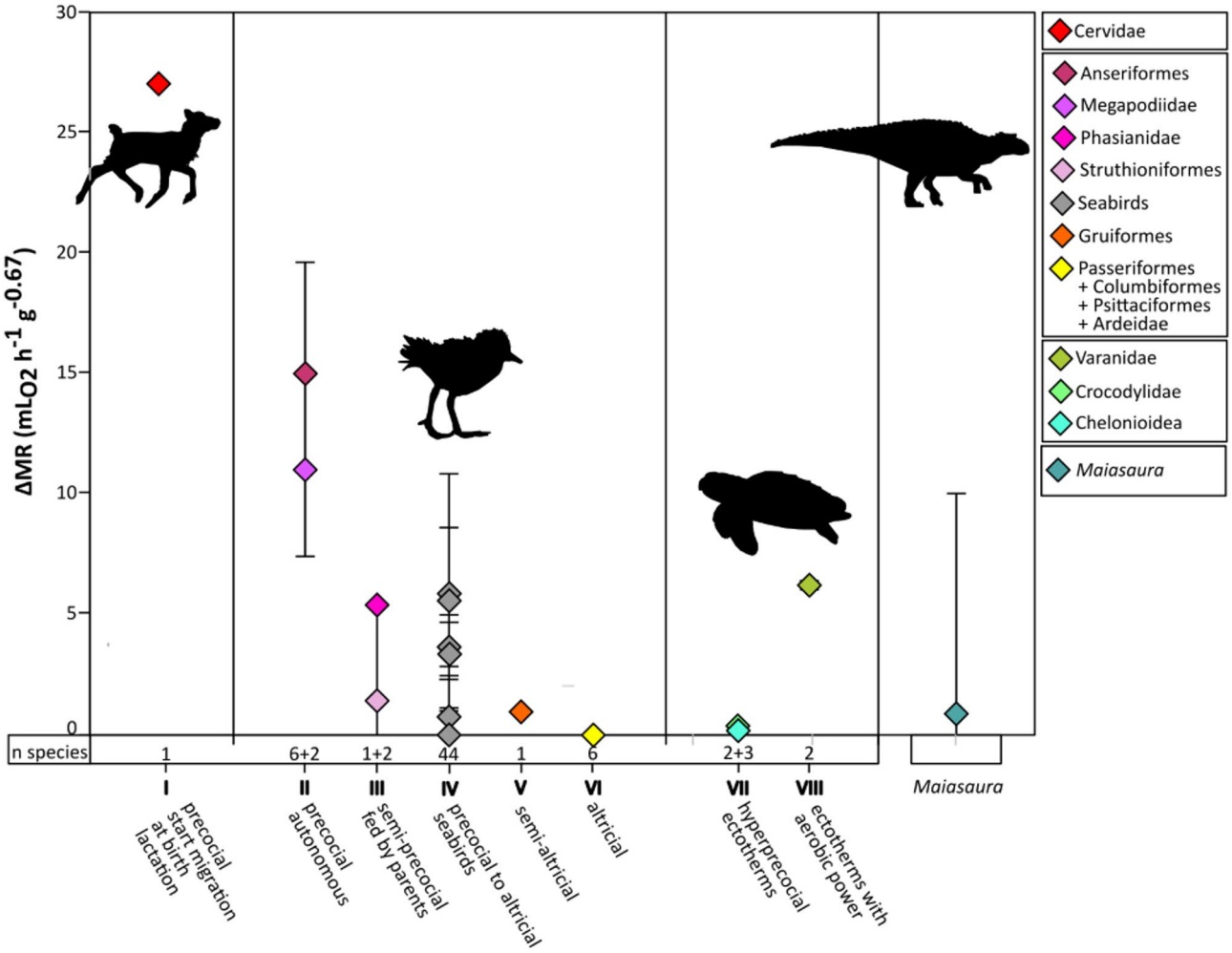

Fig. 4. Quantitative inference of the neonatal condition of *Maiasaura* comparing its ΔMR with present day tetrapods. ΔMR values is expressed in $mL(O_2).h^{-1}\ g^{-0.67}$ for different neonatal state of endotherms and ectotherms (Table 6).

model. A selection with the Holm-Sidak correction focuses on significance and controls the type I error. In this study, we therefore place more confidence in the Holm-Sidak correction selection.

Comparing the results, metabolic rates inferences are 1 $mL_{(O2)}\ h^{-1}\ g^{-0.67}$ higher utilizing the AICc selection (Table 5). In our case, this difference does not lead to major changes in the interpretations and remains smaller than the uncertainties (0→9 $mL_{(O2)}\ h^{-1}\ g^{-0.67}$). Furthermore, no differences in ΔMR values are observed (Table 5). We conclude that the mode of selection does not affect our results in our case, but this result cannot be generalized at this time. A more general and detailed comparison of these two selection methods would be necessary for further metabolic rate inferences, but it exceeds the scope of the present study.

Neonatal hadrosaur physiology

Although widespread endothermy has been proposed for Cretaceous dinosaurs including hadrosaurs from apatite oxygen isotopes[77] and diverse other proxies[78], ectothermy or low metabolic rate was proposed for hadrosaurs (1.6 $mL_{(O2)}.h^{-1}\ g^{-1}$) from the study of fossil biomolecules derived from respiration[79]. A very low RMR value of about 0.8 $mL_{(O2)}\ h^{-1}\ g^{-0.67}$ was also estimated in[25] using the PEM with the vascular canal density as a predictor variable.

In this study, we observed in *Maiasaura* femoral sections a highly vascularized cortex suggesting a high oxygen supply at rest (e.g. Fig. 2A)[23,27,31]. The associated RPOA value of 0.76 ± 0.03 is similar or higher than the RPOA values of present-day birds and mammals (0.68 in *Gallus gallus,* 0.74 in *Capreolus capreolus* and 0.81 in *Lepus europaneus*) and differs from the avascular or almost avascular bone of present-day slow-growing ectotherms having RPOA values averaging 0.015 for the two *Varanus* and 0.05 in *Crocodylus niloticus*. We inferred a neonatal RMR value for *M. peeblesorum* from $5.2_{2\rightarrow12}\ mL_{(O2)}\ h^{-1}\ g^{-0.67}$. This value is higher than that obtained in[25] for adult *M. peeblesorum* and may be explained by the difference in ontogenetic stage. Mass-specific metabolic rates are expected to decrease with ontogeny, for instance with the slowing of growth or the increasing body mass (e.g.[15]). However, comparing mass-specific RMR values of specimens having the same ontogenetic stage reduces such bias and may avoid misintinpretation of their thermophysiology. Other parameters explain the

Clade	Neonatal stage	ΔMR ($mL_{(O2)}$ h^{-1} $g^{-0.67}$)	n (species)
Data calculated from Starck and Ricklefs[15]			
Struthioniformes	Semi-precocial, fed by parents	5.4 ± 0	1
Megapodiidae	Hyperprecocial	11.0 ± 3.7	2
Phasianidae	Semi-precocial, fed by parents	$1.4_{(0- \rightarrow 5.5)}$	6
Anseriformes	Precocial	15.0 ± 4.5	6
Altricial birds (Passeriformes, Psittacidae, Scolopacidae)	Altricial	0.0 ± 0.0	10
Gruiformes	Semi-altricial	1.0 ± 0.0	1
Scolopacidae	Precocial (sea birds)	3.6 ± 1.3	11
Larinae	Semi-precocial (sea birds)	3.4 ± 1.2	11
Alcinae	Semi-precocial (sea birds)	5.9 ± 4.9	4
Sheniscidae	Semi-precocial (sea birds)	0.8 ± 0.3	3
Procellariidae	Semi-precocial (sea birds)	5.6 ± 2.9	14
Data from Gienger et al.[62] and Whitehead et al.[76]			
Crocodylus	Hyperprecocial	0.2 ± 0.0	1
Data from Jones et al.[17]			
Sea turtles	Hyperprecocial	0.4 ± 0.0	2
Data from Thompson and Withers[60]			
Varanidae	Hyperprecocial	6.2 ± 0.2	2
Data from Luick[68]			
Cervidae	Precocial	27.0 ± 0.0	1

Table 6. Neonatal ΔMR values calculated in this study using data available from the literature.

observed differences, namely: (1) the choice of the explanatory variable and (2) a different mode of eigenvector selection (Sidak method instead of AICc). This RMR value of $5.2_{2\rightarrow12}$ $mL_{(O2)}$ h^{-1} $g^{-0.67}$ is above the range of birds used in the PEM (3.8 ± 0.2 $mL_{(O2)}$ h^{-1} $g^{-0.67}$, n = 2, Table 6) and within the range of RMR values of mammals ranging from 1.5 to 15 $mL_{(O2)}$ h^{-1} $g^{-0.67}$ (n = 7, Table 6), and is higher than those of ectotherms (0.2 ± 0.2 $mL_{(O2)}$ h^{-1} $g^{-0.67}$, n = 6, Table 6). These results show that neonate *Maiasaura* rely on aerobic power at rest for growth and maintenance like extant fast-growing endotherms (Fig. 2C). It is also consistent with previous histological studies that estimated a bird-like bone apposition rate of 86.4 µm/day in nestling *M. peeblesorum*[80] and of 24 µm/day in the juvenile lambeosaurine hadrosaur *Hypacrosaurus stebingeri*[81]. Bone apposition rate of ecthotherm reptiles ranges between 0.6 and 3.5 µm/day for the lizard *Podarcis muralis* and the Nile crocodile *Crocodylus niloticus*[27]. These results also reject a varanid-like intermediate thermophysiology for hadrosaurs because monitors have relatively low bone vascularization (RPOA = 0.015) associated with low oxygen consumption rate at rest[60,82]. It is therefore more relevant to compare the *Maiasaura* ΔMR values with the endotherm ΔMR values than with the ectotherm ΔMR values for inferring their neonatal state in the altricial-precocial spectrum.

Environmental biases in the interpretation of ΔMR values

The inferred mean ΔMR value could be interpreted in terms of reproductive strategies (based on the data from[15]) or living environments because cold environments for instance increase the RMR due to higher energetic costs associated with thermoregulation, reducing ΔMR[15,16]. A continental mean annual air temperature of 16 ± 4 °C[83,84] has been determined based on a Late Cretaceous latitudinal temperature gradients reconstructed from multiple North American fossil leaf assemblages using leaf margin analysis. It is unlikely that such temperate living environment conditions could significantly affect neonatal energetic costs for thermoregulation and thermogenesis that could have increase *Maiasaura* neonatal resting metabolic rate.

Furthermore, *Maiasaura* remains and egg sites are located in the non-marine Two Medecine Formation. This 600 m-thick formation is dominated by mudstones intercalated with sandstone lenses interpreted as a vast plain, several hundred kilometers wide, situated between the Cordilleran Highlands to the west and the Interior Seaway to the east[20,85]. Such a plain does not feature environments that would require a particularly high RMR due to thermoregulation and heat production, such as cold high-altitude environments or windy coastal environments.

We reasonably assume in this study that our inferences could be interpreted in terms of reproductive strategies with negligible effect of local climatic conditions.

Since metabolic rates change throughout ontogeny (e.g.[15]), the ontogenetic stage of the specimens is also a potential source of bias, which we strive to minimize as much as possible. Regarding the present-day species used for the construction of the model inference, specimens were selected based on their age (− 1 to 4 days old, plus *Anas sp.* at 10 days old) to ensure an ontogenetic homogeneity of the datasets. Regarding *M. peeblesorum*, the ontogenetic model of the nutrient foramen presented in Fig. 1 allows for the selection of values at hatching and histology also provides access to post-hatching conditions. All these precautions ensure reliable inferences of neonatal metabolic rates.

Maiasaura neonatal state and parental care

Our novel methodology allows us to provide the first estimation of an average neonatal aerobic scope of 1 $mL_{(O2)}$ h^{-1} $g^{-0.67}$ for *M. peeblesorum*. It corresponds to the aerobic scope measured today in altricial bird neonates (Fig. 4). It can therefore be inferred that *M. peeblesorum* was altricial or semi-altricial, which means it had poor or no locomotor capacities at hatch and was dependent on parental care for feeding. This consequently suggests that it might spend its first days of life staying in the nest and that parental care was a necessity for this species.

These findings based on quantitative data are consistent with previous qualitative studies performed on poorly mineralized skeleton suggesting altriciality in *M. peeblesorum* as well as a lack of mobility. Death assemblages of *Maiasaura* individuals also suggested that the young remained in the nest for some time after hatching[9,21]. The co-occurrence of adults and juveniles at nesting sites is also supported by the occurrence of both large coprolites attributed to adults and smaller ones attributed to nestlings[86,87]. Altriciality is also consistent with the elevated growth rate of *Maiasaura* neonates, illustrated for example with a neonatal femoral apposition rate of 86.4 ± 7.9 µm/day determined from tibiae in[80]. In fact, precocial present-day birds have lower maximal growth rates than altricial birds for the same body mass at maximal growth[36]. This altricial higher growth rate might relate to parental care, which allows neonates to allocate most of their energy to growth.

Parental care is diverse, and widespread among both present-day ectothermic and endothermic terrestrial vertebrates[7,88] but it is not ubiquitous among all vertebrate species. Pre-hatching parental care in the saurolophine *Maiasaura* is evident through its nests[9], and might be widespread in hadrosaurs as we also have evidence of nesting behaviour in lambeosaurines (e.g.[21]). However, pre-hatching parental care do not necessarily induces post-hatching parental care: such behavior is observed in species of super-precocious present-day megapodes that have complex nesting strategies but do not provide parental care to neonates[89,90]. Indeed, the hadrosaur lambeosaurine *Hypacrosaurus stebingeri* also coming from the Campanian Two Medecine Formation shows differences in terms of early growth dynamics compared to *M. peeblesorum*[80,81] that might point to a different post-hatching reproductive strategy. The hypothesis of widespread post-hatching parental care in hadrosaurs deserves to be further tested and can not been confirmed yet.

Parental care duration estimate in *M. peeblesorum*

The biggest known *M. peeblesorum* specimen found in a nest has a femoral length of 130 mm (PU 22400) corresponding to a femoral mid-shaft section radius of 7.9 mm[9]. We measured its cortex thickness of 3.8 mm excluding the embryonic bone having a 4.1 mm thick radius (this study, Fig. 2A). Assuming a neonatal femoral apposition rate of 86.4 ± 7.9 µm/day determined for the tibia in Woodward et al.[80], we calculated a minimum age of 45 ± 5 days at which juveniles remain in the nest and still require parental care[9].

The youngest *M. peeblesorum* found in a non-nesting site associated with adults is a 166.4 mm-long femur (MOR 758 # 2017-04). It has a mid-shaft section radius of 10.1 mm and a cortex thickness of 6 mm corresponding to a 70-day-old juvenile with an associated uncertainty of about 5 days. We therefore estimated a nidicolous period with intensive parental care extending between 40 and 75 days for *M. peeblesorum*. *M. peeblesorum* remains longer in the nest compared to most Passeriformes that leave the nest after 2 or 3 weeks, but this duration is not aberrant compared to Accipitriformes that could remain 50 or 70 days in the nest.

Concluding remarks

We inferred the neonatal RMR and MMR values of *M. peeblesorum* from the Two Medicine Formation to evaluate its neonatal state within the altricial-precocial spectrum and the necessity of parental care after hatching. The following results are emphasized:

- Comparing the metabolic rates of specimens of different ontogenetic stages could biase interpretations because it evolves through ontogeny.
- *Maiasaura peeblesorum* mainly rely on aerobic power at rest for growth and maintenance like present-day fast-growing endotherms, distinguishing their physiology from that of ectothermic reptiles relying mostly on anaerobic power, or varanids and the leatherback turtle that use aerobic power at activity only.
- *Maiasaura peeblesorum* was most likely altricial and needed intensive parental care such as feeding and protection that long from 40 to 75 days.

Maiasaura provides a useful ecological baseline from which to infer neonatal states in other hadrosaurs of similar adult size—such as the lambeosaurine *Hypacrosaurus stebingeri*.

Indeed, this hadrosaur also coming from the Campanian Two Medecine Formation shows differences in terms of early growth dynamics compared to *M. peeblesorum*[81] that might point to a relatively more precocial condition, as inferred from differences in growth dynamics distinguishing precocial and altricial extant birds of similar adult size [36]. Overall, hadrosaur worldwide distribution and evolutionary success might be partly explained by a diversity of reproductive strategies allowing them to live and reproduce in contrasted environments during the Cretaceous.

Data availability

All data generated or analysed during this study are included in this published article (and its Supplementary Material files). 3D models are available upon request from the curators of the original collection of the specimens (*Maiasaura peeblesorum*: Museum of the Rockies; *Psittacula kameri*: les collections de Zoologie de l'Université Claude Bernard Lyon 1; *Ara ararauna*: Naturhistorisches Museum Basel; *Chelonia mydas*: les collections pédagogiques du département de Biologie de l'Ecole Normale Supérieure de Lyon; *Varanus niloticus*, *Crocodylus niloticus*, *Lepidochelys olivacea*, *Procelaria consicillata*: Museum National d'Histoire Naturelle, la collection des reptiles).

Received: 15 February 2025; Accepted: 9 June 2025
Published online: 10 July 2025

References

1. Eberhardt, L. L. Assessing the dynamics of wild populations. *J. Wildl. Manag.* **49**, 997–1012 (1985).
2. Vlad, M. O. Persistent distribution functions for the dispersion of structured populations. *Math. Biosci.* **87**, 173–198 (1987).
3. Repšys, Š & Skakauskas, V. Modelling of a one-sex age-structured population dynamics with child care. *Nonlinear Anal. Model. Control* **12**, 77–94 (2007).
4. Cubaynes, S. et al. Modeling the demography of species providing extended parental care: A capture–recapture multievent model with a case study on polar bears (*Ursus maritimus*). *Ecol. Evol.* **11**, 3380–3392 (2021).
5. Klug, H. & Bonsall, M. B. What are the benefits of parental care? The importance of parental effects on developmental rate. *Ecol. Evol.* **4**, 2330–2351 (2014).
6. Mashoodh, R., Trowsdale, A. T., Manica, A. & Kilner, R. M. Parental care shapes the evolution of molecular genetic variation. *Evol. Lett.* **7**, 379–388 (2023).
7. Horner, J. R. Dinosaur reproduction and parenting. *Annu. Rev. Earth Planet. Sci.* **28**, 19–45 (2000).
8. Meng, Q., Liu, J., Varricchio, D. J., Huang, T. & Gao, C. Parental care in an ornithischian dinosaur. *Nature* **431**, 145–146 (2004).
9. Horner, J. R. & Makela, R. Nest of juveniles provides evidence of family structure among dinosaurs. *Nature* **282**, 296–298 (1979).
10. Dong, Z.-M. & Currie, P. J. On the discovery of an oviraptorid skeleton on a nest of eggs at Bayan Mandahu, Inner Mongolia, People's Republic of China. *Can. J. Earth Sci.* **33**, 631–636 (1996).
11. Fiorillo, A. R., Hasiotis, S. T. & Kobayashi, Y. Herd structure in Late Cretaceous polar dinosaurs: A remarkable new dinosaur tracksite, Denali National Park, Alaska, USA. *Geology* **42**, 719–722 (2014).
12. Joubarne, T., Therrien, F. & Zelenitsky, D. K. Evidence of age segregation behavior in *Hypacrosaurus stebingeri* (Hadrosauridae: Lambeosaurinae) based on the taphonomic comparison of bonebeds from the Upper Cretaceous (upper Campanian) Oldman Formation of southernmost Alberta (Canada) and Two Medicine Formation of Montana (USA). *Palaeogeogr. Palaeoclimatol. Palaeoecol.* **653**, 112–416 (2024).
13. Geist, N. R. & Jones, T. D. Juvenile skeletal structure and the reproductive habits of dinosaurs. *Science* **272**, 712–714 (1996).
14. Nice, M. M. Development of behavior in precocial birds. *Trans. Linnean Soc.* **8**, 1–211 (1962).
15. Vleck, C. M. & Bucher, T. L. Energy metabolism, gas exchange, and ventilation. In *Avian Growth and Development* (eds Starck, J. M. & Ricklefs, R. E.) 89–116 (Oxford University Press, 1998). https://doi.org/10.1093/oso/9780195106084.003.0004.
16. Bakken, G. S., Williams, J. B. & Ricklefs, R. E. Metabolic response to wind of downy chicks of Arctic-breeding shorebirds (Scolopacidae). *J. Exp. Biol.* **205**, 3435–3443 (2002).
17. Jones, T. T., Reina, R. D., Darveau, C.-A. & Lutz, P. L. Ontogeny of energetics in leatherback (*Dermochelys coriacea*) and olive ridley (*Lepidochelys olivacea*) sea turtle hatchlings. *Comp. Biochem. Physiol. A: Mol. Integr. Physiol.* **147**, 313–322 (2007).
18. Seymour, R. S., Caldwell, H. R., Woodward, H. N. & Hu, Q. Growth rate affects blood flow rate to the tibia of the dinosaur *Maiasaura*. *Paleobiology* **50**(1), 1–7. https://doi.org/10.1017/pab.2023.24 (2023).
19. Dial, K. P. & Jackson, B. E. When hatchlings outperform adults: Locomotor development in Australian brush turkeys (*Alectura lathami*, Galliformes). *Proc. R. Soc. B.* **278**, 1610–1616 (2011).
20. Rogers, R. R., Horner, J. R., Ramezani, J., Roberts, E. M. & Varricchio, D. J. Updating the upper cretaceous (Campanian) two medicine formation of Montana: Lithostratigraphic revisions, new CA-ID-TIMS U-Pb ages, and a calibrated framework for dinosaur occurrences. *GSA Bull.* **137:1–2**, 315–340. https://doi.org/10.1130/B37498.1 (2024).
21. Horner, J. R. Egg clutches and embryos of two hadrosaurian dinosaurs. *J. Vertebr. Paleontol.* **19**, 607–611 (1999).
22. Cubo, J. et al. Integrative paleophysiology of the metriorhynchoid *Pelagosaurus typus* (Pseudosuchia, Thalattosuchia). *Anat. Rec.* **308**(2), 394–411. https://doi.org/10.1002/ar.25548 (2025).
23. Faure-Brac, M. G. & Cubo, J. Were the synapsids primitively endotherms? A palaeohistological approach using phylogenetic eigenvector maps. *Philos. Trans. R. Soc. B* **375**, 20190138 (2020).
24. Guénard, G., Legendre, P. & Peres-Neto, P. Phylogenetic eigenvector maps: A framework to model and predict species traits. *Methods Ecol. Evol.* **4**, 1120–1131 (2013).
25. Legendre, L. J., Guénard, G., Botha-Brink, J. & Cubo, J. Palaeohistological evidence for ancestral high metabolic rate in archosaurs. *Syst. Biol.* **65**, 989–996 (2016).
26. Sena, M. V. D. A. et al. The cost of living in Notosuchia (Crocodyliformes, Mesoeucrocodylia). *Palaeogeogr. Palaeoclimatol. Palaeoecol.* **632**, 111855 (2023).
27. Montes, L. et al. Relationships between bone growth rate, body mass and resting metabolic rate in growing amniotes: A phylogenetic approach. *Biol. J. Lin. Soc.* **92**, 63–76 (2007).
28. Montes, L., Castanet, J. & Cubo, J. Relationship between bone growth rate and bone tissue organization in amniotes: first test of Amprino's rule in a phylogenetic context. *Anim. Biol. (formerly Neth. J. Zool.)* **60**, 25–41 (2010).
29. Amprino, R. L. structure du tissu osseux envisagée comme expression de différences dans la vitesse de l'accroissement. *Arch. Biol.* **58**, 315–330 (1947).
30. Marotti, G. Static and dynamic osteogenesis. *Ital. J. Anat. Embryol.* **115:1:2**, 123–126 (2010).
31. Fleischle, C. V., Wintrich, T. & Sander, P. M. Quantitative histological models suggest endothermy in plesiosaurs. *PeerJ* **6**, e4955 (2018).
32. Ross, J. M., Fairchild, H. M., Weldy, J. & Guyton, A. C. Autoregulation of blood flow by oxygen lack. *Am. J. Physiol.-Leg. Content* **202**, 21–24 (1962).
33. Seymour, R. S., Smith, S. L., White, C. R., Henderson, D. M. & Schwarz-Wings, D. Blood flow to long bones indicates activity metabolism in mammals, reptiles and dinosaurs. *Proc. R. Soc. B.* **279**, 451–456 (2012).
34. Allan, G. H., Cassey, P., Snelling, E. P., Maloney, S. K. & Seymour, R. S. Blood flow for bone remodelling correlates with locomotion in living and extinct birds. *J. Exp. Biol.* https://doi.org/10.1242/jeb.102889 (2014).
35. Bichard, G. F. & Deeming, D. C. Chapter 9: Egg allometry: Influences of phylogeny and the altricial-precocial continuum. In *Nests, Eggs, and Incubation: New Ideas About Avian Reproduction* 97–112 (Oxford University Press, 2015).
36. Werner, J. & Griebeler, E. M. Allometries of maximum growth rate versus body mass at maximum growth indicate that non-avian dinosaurs had growth rates typical of fast growing ectothermic sauropsids. *PLoS ONE* **9**, e88834 (2014).
37. Seymour, R. S. Maximal aerobic and anaerobic power generation in large crocodiles versus mammals: Implications for dinosaur gigantothermy. *PLoS ONE* **8**, e69361 (2013).
38. R Development Core Team. R: a language and environment for statistical computing. (2008).
39. Molina-Venegas, R. et al. Assessing among-lineage variability in phylogenetic imputation of functional trait datasets. *Ecography* **41**, 1740–1749 (2018).
40. Akaike, H. Information theory and an extension of the maximum likelihood principle, in *proceedings of the Second International Symposium on Information Theory* 267–281 (1973).
41. Bauman, D., Drouet, T., Dray, S. & Vleminckx, J. Disentangling good from bad practices in the selection of spatial or phylogenetic eigenvectors. *Ecography* **41**, 1638–1649 (2018).
42. Holm, S. A simple sequentially rejective multiple test procedure. *Scand. J. Stat.* **6**(2), 65–70 (1979).
43. Šidák, Z. Rectangular confidence regions for the means of multivariate normal distributions. *J. Am. Stat. Assoc.* **62**, 626–633 (1967).

44. Shapiro, S. S. & Wilk, M. B. An analysis of variance test for normality (complete samples). *Biometrika* **52**, 591 (1965).
45. De Buffrénil, V. & Quilhac, A. Bone Tissue Types: A Brief Account of Currently Used Categories. In *de Buffrénil et al. Vertebrate Skeletal Histology and Paleohistology* https://doi.org/10.1201/9781351189590 (2021).
46. Faure-Brac, M. G., Pelissier, F. & Cubo, J. The influence of plane of section on the identification of bone tissue types in amniotes with implications for paleophysiological inferences. *J. Morphol.* **280**, 1282–1291 (2019).
47. Seymour, R. S., Hu, Q., Snelling, E. P. & White, C. R. Interspecific scaling of blood flow rates and arterial sizes in mammals. *J. Exp. Biol.* **222**(7), jeb.199554. https://doi.org/10.1242/jeb.199554 (2019).
48. Brookes, M. & Revell, W. J. *Blood Supply of Bone: Scientific Aspects*. (Springer Science & Business Media, 1998).
49. Sim, J.-H. & Ahn, D. Anatomy of the diaphyseal nutrient foramen in the long bones of the pectoral limb of German Shepherds. *Korean J. Vet. Res.* **54**, 179–184 (2014).
50. Trueta, J. The role of vessels in osteogenesis. *J. Bone Jt. Surg. Br. Vol.* **45**, 402–418 (1963).
51. Hu, Q., Nelson, T. J. & Seymour, R. S. Morphology of the nutrient artery and its foramen in relation to femoral bone perfusion rates of laying and non-laying hens. *J. Anat.* **240**, 94–106 (2022).
52. Cubo, J. & Casinos, A. Incidence and mechanical significance of pneumatization in the long bones of birds. *Zool. J. Linn. Soc.* **130**, 499–510 (2000).
53. Gutherz, S. B. & O'Connor, P. M. Postcranial skeletal pneumaticity in non-aquatic neoavians: Insights from accipitrimorphae. *J. Anat.* **241**, 1387–1398 (2022).
54. O'Connor, P. M. Evolution of archosaurian body plans: Skeletal adaptations of an air-sac-based breathing apparatus in birds and other archosaurs. *J. Exp. Zool.* **311A**, 629–646 (2009).
55. Vladimirova, I. G., Alekseeva, T. A. & Kleymenov, SYu. The dynamics of mass growth and oxygen consumption in ontogenesis of the newt *Pleurodeles waltl*: 3. The postlarval period. *Biol. Bull. Russ. Acad. Sci.* **44**, 372–378 (2017).
56. Hewison, A. J. M., Gaillard, J. M., Angibault, J. M., Van Laere, G. & Vincent, J. P. The influence of density on post-weaning growth in roe deer *Capreolus capreolus* fawns. *J. Zool.* **257**, 303–309 (2002).
57. Montes, L. et al. Relationships between bone growth rate, body mass and resting metabolic rate in growing amniotes: a phylogenetic approach. *Biol. J. Lin. Soc.* **92**, 63–76 (2007).
58. Hacklander, K., Arnold, W. & Ruf, T. Postnatal development and thermoregulation in the precocial European hare (*Lepus europaeus*). *J. Comp. Physiol. B: Biochem. Syst. Environ. Physiol.* **172**, 183–190 (2002).
59. Gilbert, C. et al. Role of huddling on the energetic of growth in a newborn altricial mammal. *Am. J. Physiol.-Regul. Integr. Comp. Physiol.* **293**, R867–R876 (2007).
60. Thompson, G. G. & Withers, P. C. Metabolic rate of neonate goannas (Squamata: Varanidae). *Comp. Biochem. Physiol. A: Mol. Integr. Physiol.* **120**, 625–631 (1998).
61. Pan, Z.-C., Ji, X., Lu, H.-L. & Ma, X.-M. Metabolic response to feeding in the Chinese striped-necked turtle, *Ocadia sinensis*. *Comp. Biochem. Physiol. Part A: Mol. Integr. Physiol.* **141**, 470–475 (2005).
62. Gienger, C. M. et al. Ontogenetic comparisons of standard metabolism in three species of crocodilians. *PLoS ONE* **12**, e0171082 (2017).
63. Stark, J. M. & Ricklefs, R. E. *Avian growth and development: evolution within the altricial-precocial spectrum* (Oxford University Press, 1998).
64. Rubner, M. Zeitschrift für Biologie, 536–562 (1883).
65. White, C. R., Cassey, P. & Blackburn, T. M. Allometric exponents do not support a universal metabolic allometry. *Ecology* **88**, 315–323 (2007).
66. Ultsch, G. R. Metabolic scaling in turtles. *Comp. Biochem. Physiol. A: Mol. Integr. Physiol.* **164**, 590–597 (2013).
67. White, C. R. & Seymour, R. S. Allometric scaling of mammalian metabolism. *J. Exp. Biol.* **208**, 1611–1619 (2005).
68. Luick, B. R. & White, R. G. Oxygen consumption for locomotion by caribou calves. *JSTOR* **50**(1), 148–152 (1986).
69. Olivier, C., Houssaye, A., Jalil, N.-E. & Cubo, J. First palaeohistological inference of resting metabolic rate in an extinct synapsid, *Moghreberia nmachouensis* (Therapsida: Anomodontia). *Biol. J. Lin. Soc.* **121**, 409–419 (2017).
70. Cubo, J., Le Roy, N., Martinez-Maza, C. & Montes, L. Paleohistological estimation of bone growth rate in extinct archosaurs. *Paleobiology* **38**, 335–349 (2012).
71. Kumar, S. et al. TimeTree 5: An expanded resource for species divergence times. *Mol. Biol. Evol.* **39**, 174 (2022).
72. Thomson, R. C., Spinks, P. Q. & Shaffer, H. B. A global phylogeny of turtles reveals a burst of climate-associated diversification on continental margins. *Proc. Natl. Acad. Sci. U.S.A.* **118**, e2012215118 (2021).
73. Prum, R. O. et al. A comprehensive phylogeny of birds (Aves) using targeted next-generation DNA sequencing. *Nature* **526**, 569–573 (2015).
74. Baker, A. J., Pereira, S. L., Haddrath, O. P. & Edge, K.-A. Multiple gene evidence for expansion of extant penguins out of Antarctica due to global cooling. *Proc. R. Soc. B.* **273**, 11–17 (2006).
75. Langer, M. C. et al. Untangling the dinosaur family tree. *Nature* **551**, E1–E3 (2017).
76. Whitehead, P. J. & Seymour, R. S. Patterns of metabolic rate in embryonic crocodilians *Crocodylus johnstoni* and *Crocodylus porosus*. *Physiol. Zool.* **63**, 334–352 (1990).
77. Amiot, R. et al. Oxygen isotopes from biogenic apatites suggest widespread endothermy in Cretaceous dinosaurs. *Earth Planet. Sci. Lett.* **246**, 41–54 (2006).
78. Legendre, L. J. & Davesne, D. The evolution of mechanisms involved in vertebrate endothermy. *Phil. Trans. R. Soc. B* **375**, 20190136 (2020).
79. Wiemann, J. et al. Fossil biomolecules reveal an avian metabolism in the ancestral dinosaur. *Nature* **606**, 522–526 (2022).
80. Woodward, H. N., Freedman Fowler, E. A., Farlow, J. O. & Horner, J. R. *Maiasaura*, a model organism for extinct vertebrate population biology: A large sample statistical assessment of growth dynamics and survivorship. *Paleobiology* **41**, 503–527 (2015).
81. Cooper, L. N., Lee, A. H., Taper, M. L. & Horner, J. R. Relative growth rates of predator and prey dinosaurs reflect effects of predation. *Proc. R. Soc. B: Biol. Sci.* **275**, 2609–2615 (2008).
82. De Buffrénil, V., Houssaye, A. & Böhme, W. Bone vascular supply in monitor lizards (Squamata: Varanidae): Influence of size, growth, and phylogeny. *J. Morphol.* **269**, 533–543 (2008).
83. Peppe, D. J. et al. Sensitivity of leaf size and shape to climate: global patterns and paleoclimatic applications. *New Phytol.* **190**, 724–739 (2011).
84. Wolfe, J. A. & Upchurch, G. R. North American nonmarine climates and vegetation during the Late Cretaceous. *Palaeogeogr. Palaeoclimatol. Palaeoecol.* **61**, 33–77 (1987).
85. Rogers, R. R. Taphonomy of three dinosaur bone beds in the Upper cretaceous two medicine formation of northwestern Montana: Evidence for drought-related mortality. *Palaios* **5**, 394–413 (1990).
86. Chin, K. The paleobiological implications of herbivorous dinosaur coprolites from the upper cretaceous two medicine formation of Montana: Why eat wood?. *Palaios* **22**, 554–566 (2007).
87. Horner, J. Evidence of colonial nesting and 'site fidelity' among ornitischian dinosaurs. *Nature* **297**, 675–676 (1982).
88. Farmer, C. G. Parental care, destabilizing selection, and the evolution of tetrapod endothermy. *Physiology* **35**, 160–176 (2020).
89. Sekercioglu, C. Megapodes: A fascinating incubation strategy. *Harvard J. Undergrad. Sci.* **5**(2), 77–83 (1999).
90. Jones, D. N. Construction and maintenance of the incubation mounds of the australian brush-turkey *Alectura lathami*. *Emu - Austral Ornithol.* **88**, 210–218 (1988).

Acknowledgements
This study was supported by the French CNRS INSU grant INTERRVIE and the European Research Executive Agency through the Marie Skłodowska-Curie Actions (MSCA) Postdoctoral Fellowship under the Project (FLAPS HORIZON-MSCA-2022-PF-01-01 n°101107135 to M. Sena). We also extend our gratitude to the Museum of the Rockies (MOR) for providing access to the fossil material, with special thanks to Eric Metz, Ellen-Therese Lamm, and John Scannella. We also acknowledge Nicolas Vidal, Caroline Tessier, Joséphine Lesur who are curators at the zoological collections of the Musée National d'Histoire Naturel (MNHN) as well as Mathilde Aladini, Stéphane Grosjean et Jérôme Courtois, the preparators; Blandine Bartschi, curator of the zoological collection at the University Claude Bernard Lyon 1 (UCBL); Maillart Margarethe, curator of the zoological collection at the Ecole Nationale Supérieure de Lyon (ENS); and Bruno Morel for providing the present-day hatchlings that enabled this study.

Author contributions
Hugo Bert wrote the main manuscript and made the figures, which were reviewed by all authors. The method was conceived by Jorge Cubo, was refined and executed by Hugo Bert and was reviewed by Mariana Sena. Hugo Bert, Holly Woodward, and John Horner contributed to the acquisition of the material, while Nicolas Rinder and Mariana Sena contributed to data acquisition. The interpretation of the data was made by Hugo Bert and was reviewed by all authors. Romain Amiot and Christophe Lécuyer contributed with the writing process.

Declarations

Competing interests
The authors declare no competing interests.

Additional information
Supplementary Information The online version contains supplementary material available at https://doi.org/10.1038/s41598-025-06282-5.

Correspondence and requests for materials should be addressed to H.B.

Reprints and permissions information is available at www.nature.com/reprints.

Publisher's note Springer Nature remains neutral with regard to jurisdictional claims in published maps and institutional affiliations.